

# ATP forms a stable complex with the essential histidine kinase WalK (YycG) domain

Reha Celikel,<sup>a‡</sup> Vidya Harini Veldore,<sup>a‡</sup> Irimpan Mathews,<sup>b</sup> Kevin M. Devine<sup>c\*</sup> and Kottayil I. Varughese<sup>a\*</sup>

<sup>a</sup>Department of Physiology and Biophysics, University of Arkansas for Medical Sciences, 4301 West Markham Street, Little Rock, AR 72205, USA, <sup>b</sup>Stanford Synchrotron Radiation Lightsource, 2575 Sand Hill Road, Menlo Park, CA 94025, USA, and <sup>c</sup>Smurfit Institute of Genetics, Trinity College Dublin, Dublin 2, Ireland

‡ These authors contributed equally to this work.

Correspondence e-mail: kdevine@tcd.ie, kivarughese@uams.edu

In *Bacillus subtilis*, the WalRK (YycFG) two-component system coordinates murein synthesis with cell division. It regulates the expression of autolysins that function in cell-wall remodeling and of proteins that modulate autolysin activity. The transcription factor WalR is activated upon phosphorylation by the histidine kinase WalK, a multi-domain homodimer. It autophosphorylates one of its histidine residues by transferring the  $\gamma$ -phosphate from ATP bound to its ATP-binding domain. Here, the high-resolution crystal structure of the ATP-binding domain of WalK in complex with ATP is presented at 1.61 Å resolution. The bound ATP remains intact in the crystal lattice. It appears that the strong binding interactions and the nature of the binding pocket contribute to its stability. The triphosphate moiety of ATP wraps around an  $Mg^{2+}$  ion, providing three O atoms for coordination in a near-ideal octahedral geometry. The ATP molecule also makes strong interactions with the protein. In addition, there is a short contact between the exocyclic O3' of the sugar ring and O2B of the  $\beta$ -phosphate, implying an internal hydrogen bond. The stability of the WalK–ATP complex in the crystal lattice suggests that such a complex may exist *in vivo* poised for initiation of signal transmission. This feature may therefore be part of the sensing mechanism by which the WalRK two-component system is so rapidly activated when cells encounter conditions conducive for growth.

Received 1 November 2011  
Accepted 29 March 2012

PDB Reference: WalK451–ATP complex, 3sl2.

## 1. Introduction

The WalRK (YycFG) two-component system (TCS) is one of only a small number of essential TCSs found in bacteria. Its distribution is restricted to Firmicutes and to some Clostridia; it is invariably found in an operon with *walJ* (*yycJ*), and with *walH* and *walI* (*yycH* and *yycI*) in the vast majority of bacteria (for a review, see Dubrac *et al.*, 2008). WalRK controls cell-wall metabolism by regulating the expression of autolysins and of proteins that modulate autolysin activity (Ahn & Burne, 2007; Bisicchia *et al.*, 2007; Dubrac *et al.*, 2007; Dubrac & Msadek, 2004; Howell *et al.*, 2003; Liu *et al.*, 2006; Ng *et al.*, 2003, 2005). Such autolysins function in murein synthesis primarily during exponential growth of *Bacillus subtilis*, when WalRK is active (Bisicchia *et al.*, 2007; Howell *et al.*, 2003). The WalK kinase localizes to the divisome in exponentially growing cells in a process requiring the PAS (Per–Arnt–Sim) domain. The activating signal emanates from its association with proteins at this location (Fig. 1; Fukushima *et al.*, 2008,

2011). The auxiliary WalH and WalI proteins exert a negative effect on WalK kinase activity through interactions between their transmembrane domains and those of WalK. These auxiliary proteins do not localize to the septum and are thought to inhibit WalK kinase activity in nondividing cells (Szurmant *et al.*, 2008). The WalJ protein is a member of the  $\beta$ -lactamase protein family and has been shown to play a role in cell-wall metabolism and in coordinating cell division and DNA replication (Biller *et al.*, 2011). Thus, the WalRK TCS and its associated WalH, WalI and WalJ proteins function to coordinate cell-wall metabolism and cell division. WalK activity is an indicator of the division status of the cell; through phosphorylation of its cognate WalR response regulator, WalK directs the expression of autolytic and other murein synthetic activities at a level commensurate with cellular requirements.

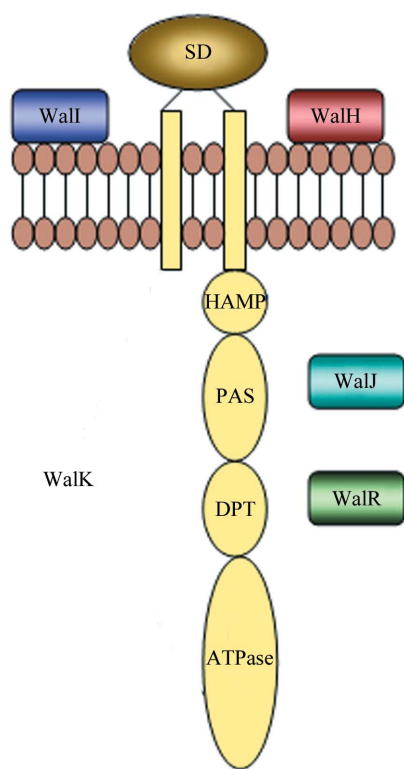


**Figure 1**

The domain organization of WalK kinase and the cellular locations of proteins in the WalRK two-component system (Fabret & Hoch, 1998). WalK is a transmembrane histidine kinase comprising 611 residues with two transmembrane domains that flank the extracellular loop domain involved in signal detection (SD; amino acids 34–183). The cytoplasmic region contains a HAMP (histidine kinases, adenyl cyclases, methyl-accepting proteins and other prokaryotic signaling proteins) domain (184–253), a PAS (Per–Arnt–Sim) domain (263–329) and an autokinase domain (376–611). The autokinase domain consists of a phosphotransferase dimerization subdomain (DPT; 376–443) containing the site of phosphorylation and the ATP-binding subdomain (488–611). The auxiliary proteins WalI and WalH are located in the cytoplasmic membrane, where they interact with the transmembrane domains of the WalK kinase, while WalJ is a  $\beta$ -lactamase-type protein that is located cytoplasmically. The response regulator WalR interacts with the DPT subdomain to exchange the phosphoryl group.

**Table 1**

Data-collection and refinement statistics for WalK451.

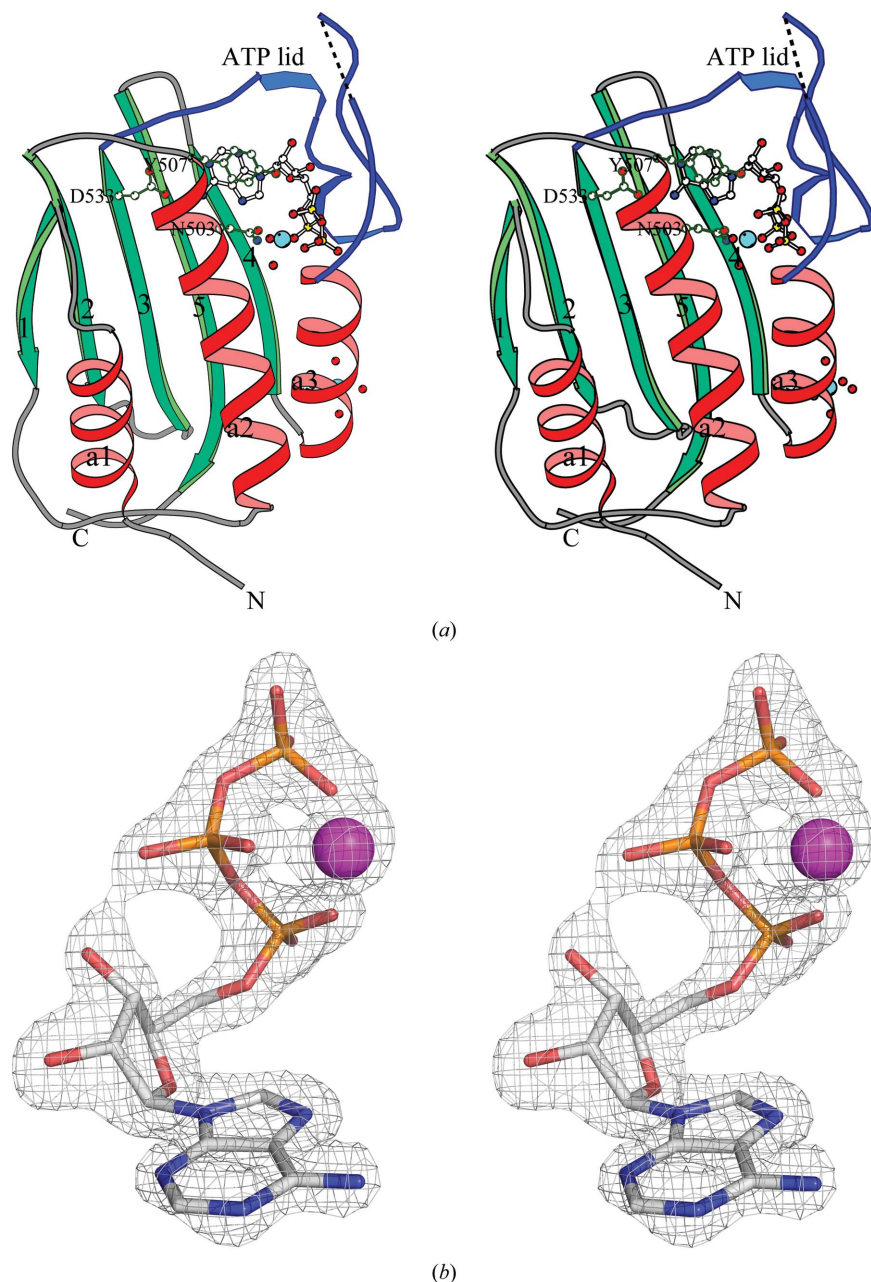
Values in parentheses are for the highest resolution shell (1.66–1.61 Å). The diffraction data were collected at 100 K using a PILATUS 6M detector on beamline 9-1 at Stanford Synchrotron Radiation Lightsource. The data were reduced using the XDS software package (Kabsch, 2010).

Data-collection statistics	
Space group	$I4_1$
Unit-cell parameters (Å, °)	$a = b = 59.040$ , $c = 99.310$ , $\alpha = \beta = \gamma = 90$
Resolution limits (Å)	28.9–1.50
No. of observations	99590 (9265)
No. of unique reflections	22011 (2036)
$R_{\text{merge}}$ (%)	2.3 (30.2)
Average $I/\sigma(I)$	36.0 (5.1)
Completeness (%)	99.8 (99.8)
Multiplicity	4.5 (4.5)
Wavelength (Å)	0.9795
No. of images	250
Crystal-to-detector distance (mm)	275
Oscillation range (°)	0.5
Refinement statistics	
Resolution limits (Å)	28.9–1.61
Average $B$ (Å <sup>2</sup> )	34.62
No. of protein atoms	188
No. of ligand atoms	31
No. of ions	2
No. of water molecules	115
$R$ factor/ $R_{\text{free}}$ †	20.7/23.4
R.m.s.d. bond lengths (Å)	0.013
R.m.s.d. bond angles (°)	1.56
Ramachandran statistics (CCP4; Winn <i>et al.</i> , 2011)	
Favored region (%)	95.7
Allowed region	3.6
Outliers	0.7
Luzzati error (Å)	0.23

† 5% of the reflections were set aside for  $R_{\text{free}}$  calculations.

WalRK is a member of the EnvZ/OmpR family of TCSs and is highly conserved in Firmicutes. Several structures of the WalRK TCS and its associated proteins have been established. The DNA-binding domain of WalR from *B. subtilis* has a winged-helix–turn–helix structure similar to that of PhoB from *Escherichia coli* and consistent with observed similarities between the WalRK and PhoPR TCSs in *B. subtilis* (Bisicchia *et al.*, 2010; Howell *et al.*, 2006; Okajima *et al.*, 2008; Trinh *et al.*, 2007). The transactivating  $\alpha 2$ – $\alpha 3$  domain of WalR is larger than PhoB and is proposed to interact with the sigma factor attached to RNA polymerase. Bent *et al.* (2004) have established the structure of the receiver domain of RR02 (a WalR ortholog) from *Streptococcus pneumoniae*, showing it to be similar to the receiver domains of the OmpR/PhoB family of response regulators. The WalH and WalI structures have been established and a model has been proposed for the interaction between their transmembrane domains and those of the WalK kinase (Santelli *et al.*, 2007; Surmant *et al.*, 2006, 2008).

As a part of our program to structurally characterize the WalRK TCS, we report here the crystal structure of the ATP-binding domain of WalK (WalK451; residues 451–611) using 1.61 Å resolution diffraction data. The ATP-binding domain is also called the catalytic ATP-binding (CA or cat) domain (Dutta & Inouye, 2000). We will call this domain simply the ATP domain.

**Figure 2**

Crystal structure of WalK451. (a) A stereoview of a cartoon diagram of the structure of the WalK ATP domain in complex with ATP is depicted. The domain adopts an  $\alpha/\beta$ -sandwich fold, with the lower layer formed by a  $\beta$ -sheet comprising five  $\beta$ -strands (green) labeled 1, 2, 3, 5 and 4 and the upper layer consisting of three  $\alpha$ -helices (red) labeled  $\alpha 1$ ,  $\alpha 2$  and  $\alpha 3$ . The loop regions are shown in grey. A large flexible loop (residues Glu534–Gly567), termed the ATP lid, is shown in blue. Three missing residues (Thr558–Lys560) are represented by dotted lines. ATP is shown as a ball-and-stick model. A  $\text{Mg}^{2+}$  ion (cyan) is coordinated to ATP. The side chains of three residues that make prominent interactions with the ATP are also shown in ball-and-stick representation. Asn503 participates in  $\text{Mg}^{2+}$  coordination. Asp533 forms a hydrogen bond to the adenine ring. The aromatic side chain of Tyr507 stacks close to the adenine ring. A second  $\text{Mg}^{2+}$  ion is located near the C-terminal portion of helix  $\alpha 3$ . This ion sits on a crystallographic twofold symmetry axis and bridges two neighboring protein molecules in the crystal lattice. The cation is coordinated by three water molecules that interact with one protein molecule and their symmetry equivalents that interact with the other molecule. Therefore, this  $\text{Mg}^{2+}$  ion plays a role in the crystal packing. The figure was produced using the program *BobScript* (Esnouf, 1997). (b) A  $2F_o - F_c$  map showing the electron density for the ATP and the  $\text{Mg}^{2+}$  ion. The contours are drawn at the  $3.0\sigma$  level. The density for the  $\gamma$ -phosphate is as strong as the density for the  $\alpha$ -phosphate or the  $\beta$ -phosphate. O atoms are shown in red, N atoms in blue, P atoms in yellow and Mg atoms in magenta. The figure was generated using *PyMOL* (<http://www.pymol.org>).

## 2. Experimental

### 2.1. Protein expression and purification

The ATP domain of WalK was amplified with primers YycG\_451 (5'-GGGAATTCCATATGtggttcagattgtccggtttatg-3') and YycG\_RKI (5'-GGGAATTC-CATATGtggttcagattgtccggtttatg-3') using chromosomal DNA as a template. The amplified DNA fragment (527 bp) and the pET21b expression vector were each digested with *XhoI* and *NdeI*, ligated and transformed into *E. coli* strain TG1. Plasmid HA110 was isolated from the resultant transformants and the DNA insert encoding WalK451 was verified by sequencing. Plasmid HA110 was transformed into *E. coli* expression strain BL21 (DE3) to give strain HA80. Expression and purification of the WalK451 protein was performed as described previously (Howell *et al.*, 2006). The purified protein was dialysed and stored in buffer containing glycerol [20 mM Tris-HCl pH 8, 0.3 M NaCl, 50% (v/v) glycerol].

### 2.2. Crystallization and data collection

Crystals of the WalK451–ATP complex were grown using the hanging-drop vapor-diffusion technique. A  $7 \text{ mg ml}^{-1}$  protein stock was prepared in a solution consisting of 10 mM Tris-HCl, 100 mM NaCl, 5% glycerol and 1.5 mM  $\text{NaN}_3$  at pH 7.5. 100  $\mu\text{l}$  ATP stock solution at a concentration of 500 mM was prepared using 1 M Tris-HCl pH 9. As ATP is very acidic in nature, when the required amount of ATP to make this solution was dissolved in 1 M Tris-HCl pH 9 the final pH of the ATP solution was 6.5. ATP stock solution was combined with the protein stock to give a final concentration of 10 mM. This was followed by addition of 1 M  $\text{MgCl}_2$  to the protein–ATP mixture to give a concentration of 40 mM. Crystals were obtained from drops consisting of 2  $\mu\text{l}$  protein–ATP– $\text{MgCl}_2$  complex and 1  $\mu\text{l}$  reservoir solution (80 mM dibasic ammonium tartrate and 8% polyethylene glycol 3350 at pH 6.5). The crystals grew to average dimensions of  $0.2 \times 0.3 \times 0.5 \text{ mm}$  in about three weeks in an incubator at 287 K. The initial data were collected to a resolution of  $2.8 \text{ \AA}$  using an RU-H3R/R-AXIS IV<sup>++</sup> system in our laboratory; high-resolution data ( $1.61 \text{ \AA}$ ) were subsequently collected at the Stanford Synchrotron Radiation Light-source (Table 1).

### 2.3. Structure solution and refinement

The structure was solved by molecular-replacement techniques using the ATP domain of HK853 (Marina *et al.*, 2005; PDB entry 2c2a) as a search model with the program *CNS* (Brünger *et al.*, 1998). Model building was carried out using the program *O* (Jones *et al.*, 1991). After several cycles of model building and refinement using the program *REFMAC5* (Murshudov *et al.*, 2011), the structure refined to a final *R* and *R*<sub>free</sub> of 20.7% and 23.4%, respectively. Data-collection and refinement statistics are provided in Table 1.

## 3. Results

### 3.1. Description of the structure

The final model comprises 145 protein residues, an ATP molecule, 115 water molecules and two Mg<sup>2+</sup> ions. Two residues in a loop (472 and 473), six residues in another loop (555–560) and nine residues at the C-terminus of the molecule (603–611) were not visible in the electron-density maps. The protein sequence has an additional 15 residues at the C-terminus constituting a TEV protease site and a hexahistidine tag, but these residues were also not located. Fig. 2(a) depicts a ribbon representation of the WalK ATP domain (WalK451). A sequence comparison of WalK451 and the search model HK853 shows that there is 38% sequence identity between them. The overall folds of the two structures are similar, but there are some large variations in the connecting loop regions. The structure is made up of a two-layer  $\alpha/\beta$ -sandwich fold with a large ATP pocket at the top. The bottom layer is a  $\beta$ -sheet comprising five  $\beta$ -strands. Strands 1 and 2 run parallel, while strands 2, 3, 5 and 4 alternate in direction. The top layer is made up of three  $\alpha$ -helices. There is a large flexible loop (Asp534–Gly567) containing a short helical segment that is crucially involved in ATP binding. This region can undergo major conformational changes upon binding to ATP and is designated the ATP lid (Dutta & Inouye, 2000). The protein fold is characteristic of the ATP domains of histidine kinases and is unrelated to the fold of mammalian ATP-binding domains (Tanaka *et al.*, 1998). The specific fold is termed a Bergerat fold and is found in three other seemingly unrelated families, namely gyrase, Hsp90 and MutL (Dutta & Inouye, 2000; Gao *et al.*, 2007). In conventional NTPase domains a central  $\beta$ -sheet is sandwiched between two layers of  $\alpha$ -helices, unlike the Bergerat fold which has only two layers. The ATP molecule is bound tightly to the protein, as indicated by the strong electron density for ATP (Fig. 2b). The ATP molecule is involved in several interactions with the protein molecule, solvent molecules and the Mg<sup>2+</sup> ion. In addition to direct interactions with the protein molecule, it makes bridging interactions through the Mg<sup>2+</sup> ion and a number of solvent molecules. Various interactions of ATP, starting with the magnesium coordination, will be discussed below.

### 3.2. ATP and Mg<sup>2+</sup> coordination

The triphosphate moiety of ATP contributes three of the six O atoms that coordinate to the Mg<sup>2+</sup> ion. The O atoms O1A,

O1B and O1G attached to the three P atoms PA, PB and PG, respectively, are coordinated to magnesium (Fig. 3a). Additionally, two water molecules and the side-chain O atom OD1 of Asn503 also are coordinated to the magnesium, with nearly ideal coordination geometry.

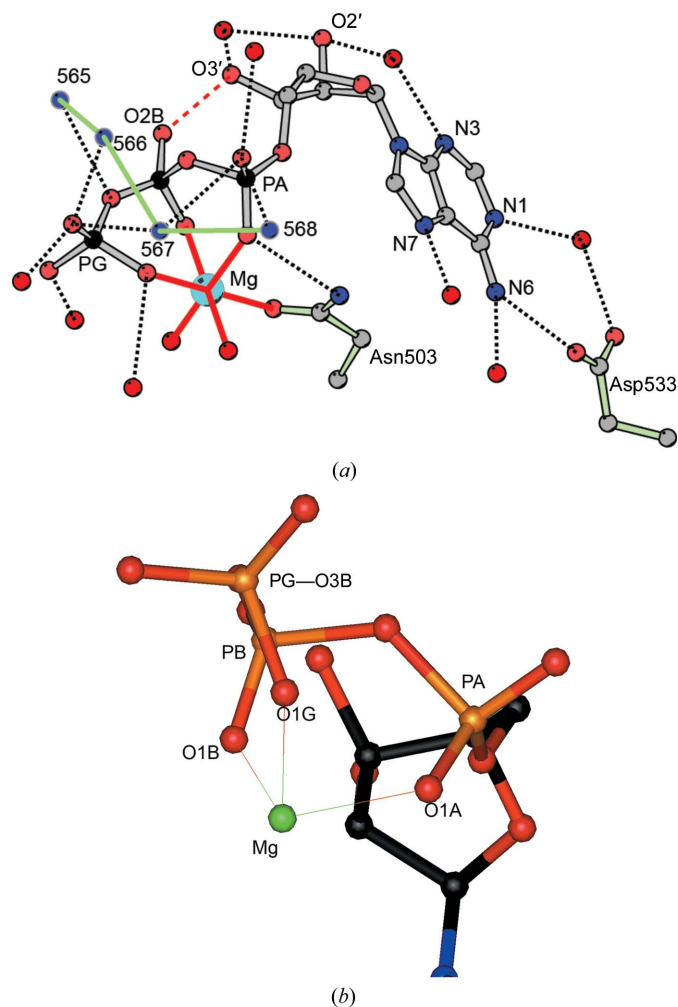


**Figure 3**

Mg<sup>2+</sup> coordination to ATP (WalK). (a) Interactions of ATP with its environment. The magnesium ion is coordinated by six O atoms (represented by thick red lines). Three O atoms from the triphosphate moiety, two water molecules and the side-chain O atom of Asn503 are coordinated to magnesium in an octahedral geometry with coordination distances close to 2.0 Å (1.9–2.1 Å). Hydrogen bonds are represented by dotted lines. In addition to coordinating to magnesium, the side chain of Asn503 makes a hydrogen-bonding interaction with the triphosphate moiety. Asp533 makes a direct hydrogen bond to N6 of the adenine ring. Tyr507 stacks near the adenine ring and makes a weak hydrogen bond (not shown) to a phosphate O atom. In addition, the main-chain amides of Gly565, Leu566, Gly567 and Leu568 (shown as blue circles and linked by green lines) are hydrogen-bond donors to ATP. There is a possible strong internal hydrogen bond between O3', the exocyclic O atom of the sugar ring, and the phosphate O atom O2B, with an O...O distance of 2.47 Å (shown as a red dashed line). Eight water molecules make direct hydrogen bonds to ATP and most of them are linked to the protein *via* hydrogen bonds. O atoms are shown in red, N atoms in blue, C atoms in white, P atoms in black and Mg atoms in cyan. (b) A view of a projection down the PG–O3B bond, showing the eclipsed conformation.



### 3.3. Hydrogen bonds

The O atoms of the triphosphate make a number of strong hydrogen-bonding interactions with water molecules. It should be pointed out that all three of the terminal O atoms attached to the  $\gamma$ -phosphate P atom PG make strong interactions. As mentioned above, O1G is coordinated to the Mg atom, O2G makes a strong hydrogen bond to a solvent molecule (2.51 Å) and O3G is the acceptor of two N—H...O hydrogen bonds from the backbone amide N atoms of Leu566 and Gly567 (Fig. 3*a*). This glycine-rich portion of the peptide wraps around the O3G atom such that the two amide H atoms point towards it. Another amide, from Gly565, interacts with O3B.

The adenine ring of ATP makes both hydrophilic and hydrophobic interactions. The N atoms N7, N6, N1 and N3 make strong hydrogen-bonding interactions with water molecules. One of the carboxyl O atoms of Asp533 forms a hydrogen bond to N6, while the other O atom has a bridging interaction through a water molecule to N1. The aromatic ring of Tyr507 and the side chain of Ile538 are positioned on opposite sides of the adenine ring, but with a shift towards the edge of the adenine ring. Both of the exocyclic O atoms O2' and O3' of the sugar ring make hydrogen bonds to water molecules. The water molecule that interacts with N3 of the adenine ring makes another strong hydrogen bond to O2'. Another water molecule interacts with both O2' and O3'. The intramolecular distance between O3' and O2B is 2.47 Å, suggesting the possibility of a strong internal hydrogen bond with O3' as the proton donor and O2B as the proton acceptor.

### 3.4. A second Mg<sup>2+</sup> ion

In addition to the magnesium ion attached to the ATP molecule, there is a second magnesium ion in the lattice which does not bind to ATP or to the protein molecule directly (Fig. 2*a*). It sits on a crystallographic twofold axis and coordinates to six water molecules: Ow1, Ow2 and Ow3 and their symmetry equivalents. The water molecules Ow1 and Ow3 form strong hydrogen bonds to the carboxylate of Asp581, while Ow2 forms strong hydrogen bonds to the carbonyls of Gly580 and Gln576 (not shown). Therefore, the magnesium ion plays a role in the crystal packing, mediating interactions between two symmetry-related protein molecules.

## 4. Discussion

The solution structure of an ATP domain of EnvZ has been determined by NMR (Tanaka *et al.*, 1998). A few crystal structures of ATP domains from histidine kinases in complex with ATP analogs have been reported; for example, PhoQ (Marina *et al.*, 2001), CheA (Bilwes *et al.*, 2001) and HK853 (Marina *et al.*, 2005). Several crystal structures of apo forms have also been documented (Bilwes *et al.*, 1999; Nowak *et al.*, 2006; Song *et al.*, 2004), but to date only the structure of the DesK ATP-binding domain in complex with ATP has been reported (Trajtenberg *et al.*, 2010). The overall structures are similar, but the conformation of the ATP lid varies widely, as discussed later.

### 4.1. Mg<sup>2+</sup> coordination

The ATP molecule assumes a suitable conformation for coordination to the Mg<sup>2+</sup> ion (Fig. 3*a*). The triphosphate moiety of ATP wraps around the Mg<sup>2+</sup> ion to provide three O atoms for coordination. Fig. 3(*b*) shows a projection of the triphosphate tail of the molecule down the PG—O3B bond. Instead of taking up the energetically more favorable staggered conformation, the molecule assumes an eclipsed conformation which allows ATP to adopt a proper coordination geometry for Mg<sup>2+</sup>. The coordination geometry is close to ideal, with all six coordination distances having values of less than 2.1 Å.

### 4.2. Interactions of the phosphoryl O atoms

The ATP molecule additionally takes part in a number of strong hydrogen-bonding interactions directly or indirectly to the protein. For example, all three terminal O atoms attached to the  $\gamma$ -phosphate have strong interactions which are likely to contribute to the stability. In addition, the O3'...O2B distance of 2.47 Å and the C3'—O3'...O2A angle of 109° suggest the prospect of a strong internal hydrogen bond between the sugar moiety and the phosphate group.

### 4.3. ATP is stable in the crystal lattice

WalRK signaling involves transfer of the phosphoryl group from ATP bound to the C-terminal domain to a histidine residue in the DPT domain of WalK and subsequent transfer to an aspartate residue in the response regulator WalR. In the current analysis, even though the DPT domain is absent, ATP can still lose the  $\gamma$ -phosphate owing to hydrolysis. Because of this possibility, crystallographic analyses of similar domains are generally carried out using ATP analogues rather than ATP itself. One of the most interesting aspects of this study is that the natural substrate ATP forms a stable complex, as found in the crystal structure of the DesK kinase ATP domain (Trajtenberg *et al.*, 2010). A comparison of the two structures shows that the ATP conformation and the Mg<sup>2+</sup> coordination are very similar in the two structures. Both of these structures are characterized by near-ideal octahedral geometry for Mg<sup>2+</sup> coordination in which three of the six O atoms are contributed by an ATP molecule. In WalK451, two coordinating atoms are from solvent water molecules and the sixth coordinating atom is from the side chain of an asparagine residue, whereas in DesK only one O atom is from the solvent and the other two are from the side chains of Asn and Gln residues. Both structures show the prospect of internal hydrogen bonds. It appears that the mode of Mg<sup>2+</sup> coordination, strong binding interactions with the protein and an internal hydrogen bond could be contributing to the stability of the ATP molecules in WalK and DesK.

It is difficult to provide a compelling explanation for the stability of ATP in the crystal lattice. If the binding of ATP in the pocket shields the  $\gamma$ -phosphate from the approach of a water molecule, hydrolysis can be avoided. In the WalK451–ATP complex there are water molecules in the vicinity of PG, but none of them are properly positioned to make a nucleo-

philic attack on the  $\gamma$ -phosphate. Thus, while the protein does not shield PG from the solvent completely, it appears to produce an environment that is unfavorable for hydrolysis.

The stability of the WalK–ATP complex is intriguing. It may be that such a complex exists *in vivo* poised for autophosphorylation upon receipt of signals sensed by the loop of intracellular PAS domains. This unusual feature may therefore be part of the sensing mechanism by which the WalRK two-component system is so rapidly activated when cells encounter growth-conducive conditions (Botella *et al.*, 2011).

#### 4.4. Comparison with other ATP-binding domains

Fig. 4 depicts a superposition of WalK451 with two representative ATP domains: those of PhoQ (Marina *et al.*, 2001) and DesK. The overall conformation of all three domains is very similar, but the ATP lids show significant differences, varying in length and conformation. The ATP lids of WalK and PhoQ are longer compared with that of DesK and comprise 34 and 30 residues, respectively. The ATP lid in DesK is much tighter, consisting of only 15 residues. The ATP domains in histidine kinases have certain conserved sequence segments known as the N, D, G1, F and G2 boxes (Dutta & Inouye, 2000; Parkinson & Kofoed, 1992; Swanson *et al.*, 1994). Asn503, belonging to the N box, is involved in  $Mg^{2+}$  coordination. Asp533 of the D box interacts with N6 of the adenine

ring of ATP. This residue has been implicated in providing specificity for ATP over GTP (Dutta & Inouye, 2000). The G1 box (Gly535–Gly537) forms part of the adenine-binding pocket. Phe547 of the F box is located near the  $\gamma$ -phosphate of ATP, but the side chain is more than 8 Å away from the ATP and makes no contacts with it. There are two other aromatic residues Phe550 and Tyr551 downstream from this residue, but they are also located too far away from ATP to make any interactions. Interestingly, the aromatic residue that stacks with the adenine ring is Tyr507, four residues downstream from the N box. Residues Gly562–Gly567 form the G2 box. The amides of Gly565, Leu566, Gly567 and Leu568 interact with the triphosphate moiety of ATP (Fig. 3*a*). Therefore, the conserved boxes are either involved in direct interactions with ATP or in the formation of the ATP-binding pocket.

#### 5. Conclusion

This analysis shows that WalK451 has a similar conformation to the corresponding domains in other histidine kinases. The protein fold comprises two layers: one made up of a  $\beta$ -sheet and the other made up of  $\alpha$ -helices with an ATP pocket at the top. A comparison with other domains shows that the  $\beta$ -sheets exhibit considerable similarity but that the orientations of the helices in the other layer can have larger differences. The most dramatic difference is seen in the ATP lid, a large loop that

embraces the ATP molecule. Flexibility of this loop is necessary for binding ATP and interacting with the phosphotransferase domain to transfer the phosphoryl group to the histidine residue and release ADP. The most fascinating aspect of the structure is that the ATP molecule was not hydrolyzed and remained intact during crystallization and data collection. ATP adopts a suitable conformation to have excellent coordination geometry with  $Mg^{2+}$  and to have very favorable interactions at the binding pocket, generating an environment that is unfavorable for hydrolysis of the phosphoryl group.

This work was supported in part by the Arkansas Bioscience Institute. The diffraction data were collected at the Stanford Synchrotron Radiation Lightsource (SSRL). SSRL is a national user facility operated by Stanford University on behalf of the US Department of Energy, Office of Basic Energy Sciences. The SSRL Structural Molecular Biology Program is supported by the Department of Energy, Office of Biological and Environmental Research and by the National Institutes of Health, National Center for Research Resources, Biomedical Technology Program and the National Institute of General Medical Sciences. Work

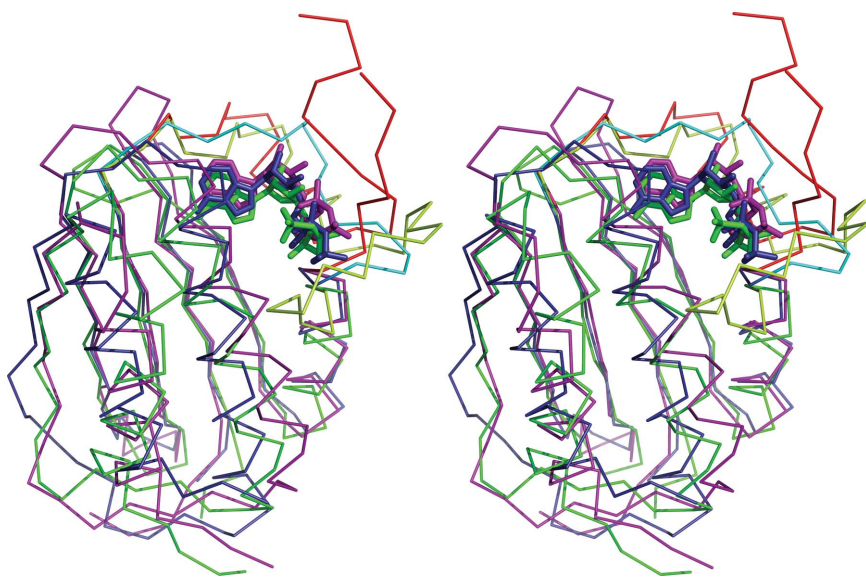


**Figure 4**

A stereoview showing a comparison of the ATP domains of WalK (purple), DesK (deep blue) and PhoQ (green). The figure was generated by superposing the  $\beta$ -strand residues (473–451, 512–520, 526–534, 580–585 and 590–598) of WalK onto the corresponding residues of DesK (r.m.s.d. = 1.1 Å) and PhoQ (r.m.s.d. = 0.9 Å). The overall conformations of the three domains are very similar. The ATP lids, however, differ in length and conformation and are colored differently from the rest of the molecule. The ATP lids in WalK (shown in red; Glu524–Gly567) and PhoQ (shown in light green; Asp416–Gly445) comprise 30 residues or more, while that in DesK (shown in cyan; Asp321–His335) is only half the size. The conformations of ATP in WalK and DesK are very similar, but the AMPPNP conformation in PhoQ has significant differences. The figure was generated using PyMOL (<http://www.pymol.org>).

at the Devine laboratory was supported by SFI Principal Investigator Award 08/IN.1/B1859.

## References

- Ahn, S.-J. & Burne, R. A. (2007). *J. Bacteriol.* **189**, 6293–6302.
- Bent, C. J., Isaacs, N. W., Mitchell, T. J. & Riboldi-Tunnicliffe, A. (2004). *J. Bacteriol.* **186**, 2872–2879.
- Billar, S. J., Wayne, K. J., Winkler, M. E. & Burkholder, W. F. (2011). *J. Bacteriol.* **193**, 896–908.
- Bilwes, A. M., Alex, L. A., Crane, B. R. & Simon, M. I. (1999). *Cell*, **96**, 131–141.
- Bilwes, A. M., Quezada, C. M., Croal, L. R., Crane, B. R. & Simon, M. I. (2001). *Nature Struct. Biol.* **8**, 353–360.
- Bisicchia, P., Lioliou, E., Noone, D., Salzberg, L. I., Botella, E., Hübner, S. & Devine, K. M. (2010). *Mol. Microbiol.* **75**, 972–989.
- Bisicchia, P., Noone, D., Lioliou, E., Howell, A., Quigley, S., Jensen, T., Jarmer, H. & Devine, K. M. (2007). *Mol. Microbiol.* **65**, 180–200.
- Botella, E., Hübner, S., Hokamp, K., Hansen, A., Bisicchia, P., Noone, D., Powell, L., Salzberg, L. I. & Devine, K. M. (2011). *Microbiology*, **157**, 2470–2484.
- Brünger, A. T., Adams, P. D., Clore, G. M., DeLano, W. L., Gros, P., Grosse-Kunstleve, R. W., Jiang, J.-S., Kuszewski, J., Nilges, M., Pannu, N. S., Read, R. J., Rice, L. M., Simonson, T. & Warren, G. L. (1998). *Acta Cryst. D* **54**, 905–921.
- Dubrac, S., Bisicchia, P., Devine, K. M. & Msadek, T. (2008). *Mol. Microbiol.* **70**, 1307–1322.
- Dubrac, S., Boneca, I. G., Poupel, O. & Msadek, T. (2007). *J. Bacteriol.* **189**, 8257–8269.
- Dubrac, S. & Msadek, T. (2004). *J. Bacteriol.* **186**, 1175–1181.
- Dutta, R. & Inouye, M. (2000). *Trends Biochem. Sci.* **25**, 24–28.
- Esnouf, R. M. (1997). *J. Mol. Graph.* **15**, 133–138.
- Fabret, C. & Hoch, J. A. (1998). *J. Bacteriol.* **180**, 6375–6383.
- Fukushima, T., Furihata, I., Emmins, R., Daniel, R. A., Hoch, J. A. & Szurmant, H. (2011). *Mol. Microbiol.* **79**, 503–522.
- Fukushima, T., Szurmant, H., Kim, E. J., Perego, M. & Hoch, J. A. (2008). *Mol. Microbiol.* **69**, 621–632.
- Gao, R., Mack, T. R. & Stock, A. M. (2007). *Trends Biochem. Sci.* **32**, 225–234.
- Howell, A., Dubrac, S., Andersen, K. K., Noone, D., Fert, J., Msadek, T. & Devine, K. (2003). *Mol. Microbiol.* **49**, 1639–1655.
- Howell, A., Dubrac, S., Noone, D., Varughese, K. I. & Devine, K. (2006). *Mol. Microbiol.* **59**, 1199–1215.
- Jones, T. A., Zou, J.-Y., Cowan, S. W. & Kjeldgaard, M. (1991). *Acta Cryst. A* **47**, 110–119.
- Kabsch, W. (2010). *Acta Cryst. D* **66**, 133–144.
- Liu, M., Hanks, T. S., Zhang, J., McClure, M. J., Siemsen, D. W., Elser, J. L., Quinn, M. T. & Lei, B. (2006). *Microbiology*, **152**, 967–978.
- Marina, A., Mott, C., Auyzenberg, A., Hendrickson, W. A. & Waldburger, C. D. (2001). *J. Biol. Chem.* **276**, 41182–41190.
- Marina, A., Waldburger, C. D. & Hendrickson, W. A. (2005). *EMBO J.* **24**, 4247–4259.
- Murshudov, G. N., Skubák, P., Lebedev, A. A., Pannu, N. S., Steiner, R. A., Nicholls, R. A., Winn, M. D., Long, F. & Vagin, A. A. (2011). *Acta Cryst. D* **67**, 355–367.
- Ng, W.-L., Robertson, G. T., Kazmierczak, K. M., Zhao, J., Gilmour, R. & Winkler, M. E. (2003). *Mol. Microbiol.* **50**, 1647–1663.
- Ng, W.-L., Tsui, H.-C. T. & Winkler, M. E. (2005). *J. Bacteriol.* **187**, 7444–7459.
- Nowak, E., Panjikar, S., Morth, J. P., Jordanova, R., Svergun, D. I. & Tucker, P. A. (2006). *Structure*, **14**, 275–285.
- Okajima, T., Doi, A., Okada, A., Gotoh, Y., Tanizawa, K. & Utsumi, R. (2008). *FEBS Lett.* **582**, 3434–3438.
- Parkinson, J. S. & Kofoed, E. C. (1992). *Annu. Rev. Genet.* **26**, 71–112.
- Santelli, E., Liddington, R. C., Mohan, M. A., Hoch, J. A. & Szurmant, H. (2007). *J. Bacteriol.* **189**, 3290–3295.
- Song, Y., Peisach, D., Pioszak, A. A., Xu, Z. & Ninfa, A. J. (2004). *Biochemistry*, **43**, 6670–6678.
- Swanson, R. V., Alex, L. A. & Simon, M. I. (1994). *Trends Biochem. Sci.* **19**, 485–490.
- Szurmant, H., Bu, L., Brooks, C. L. & Hoch, J. A. (2008). *Proc. Natl Acad. Sci. USA*, **105**, 5891–5896.
- Szurmant, H., Zhao, H., Mohan, M. A., Hoch, J. A. & Varughese, K. I. (2006). *Protein Sci.* **15**, 929–934.
- Tanaka, T., Saha, S. K., Tomomori, C., Ishima, R., Liu, D., Tong, K. I., Park, H., Dutta, R., Qin, L., Swindells, M. B., Yamazaki, T., Ono, A. M., Kainosho, M., Inouye, M. & Ikura, M. (1998). *Nature (London)*, **396**, 88–92.
- Trajtenberg, F., Graña, M., Ruétalo, N., Botti, H. & Buschiazzi, A. (2010). *J. Biol. Chem.* **285**, 24892–24903.
- Trinh, C.-H., Liu, Y., Phillips, S. E. V. & Phillips-Jones, M. K. (2007). *Acta Cryst. D* **63**, 266–269.
- Winn, M. D. *et al.* (2011). *Acta Cryst. D* **67**, 235–242.